Available online at www.sciencedirect.com
ScienceDirect
Trans. Nonferrous Met. Soc. China 33(2023) 396−408
Transactions of Nonferrous Metals Society of China
www.tnmsc.cn

# Effect of Ca and rotation speed on microstructure and solidification parameters of AZ91 magnesium alloy produced by semi-solid casting through rotating container process

Saeed G. SHABESTARI, Ehsan GHANIABADI

School of Metallurgy and Materials Engineering,
Iran University of Science and Technology, 1684613114 Tehran, Iran

Received 23 October 2021; accepted 23 February 2022

**Abstract:** Microstructure of AZ91 magnesium alloy was modified by using semi-solid rotating container process (RCP) and addition of 1 wt.% Ca. Thermal analysis (CA-CCTA) was performed during semi-solid process in order to determine the relationship between microstructural modification and RCP parameters. The container containing molten AZ91 alloy was rotated by rotation speed of 0, 150, 180 and 210 r/min at 640−580 °C. The cooling curves were plotted to determine the solidification characteristics, solid fraction and dendrite coherency point (DCP). The results indicated that the cooling rate increased with increasing the rotation speed significantly and led to an increase in maximum solidification range of 15.9 and 6.4 °C for AZ91 and AZ91−1Ca (wt.%), respectively. Applying shear force to the slurry at 180 r/min minimized the solid fraction and delayed appearance of DCP. It affected the microstructure characteristics such as grain size and circularity factor. The rotation of 180 r/min at 585 °C resulted in the globular microstructure with a circularity factor of 0.72 and a grain size of 73.4 μm. The addition of 1 wt.% Ca to AZ91 in the optimum condition of RCP increased the circularity factor to 0.81 and reduced the grain size to 53.2 μm.

**Key words:** semi-solid; magnesium alloy; thermal analysis; shearing force; globular structure

## 1 Introduction

Magnesium alloys have a comprehensive usage in automobile, aerospace and portable, because of their high specific strength, excellent damping characteristics, good castability, and recyclability [1]. Magnesium as a pure metal has limited applications. Alloying elements such as aluminum, zinc, manganese, calcium, zirconium, and rare earth elements improve the mechanical strength and corrosion resistance [2−6].

The effect of Ca on magnesium alloys includes increasing high-temperature mechanical properties, reducing the viscosity of the melt, reducing oxidation of the melt, and improving the heat treatment capability [7]. The presence of Ca up to 0.5 wt.% does not cause significant changes in the microstructure of AZ91 alloy and only modifies dendritic cells and $Mg_{17}Al_{12}$ phases. However, increasing the content of Ca reduces the amount of $\beta$-phase whereas in AZ91−4Ca, it is completely removed from the microstructure [8]. The results of other studies [5,9] also show that Ca up to 1 wt.% has a great effect on the grain size of AZ91 alloy, but its effect is reduced at higher contents.

Semi-solid casting methods are developed to achieve superior mechanical and physical properties. This process improves the microstructure and forms a non-dendritic or globular morphology in the alloy during the casting stage [10,11] Swirled enthalpy equilibration device (SEED) is a novel method which presents the field of semi-solid casting of light alloys such as magnesium and aluminum [12,13].

**Corresponding author:** Saeed G. SHABESTARI, E-mail: shabestari@iust.ac.ir
DOI: 10.1016/S1003-6326(22)66115-6

In this method a superheated alloy is poured into a cylindrical mold which is rotated off-center at a certain rotation speed [12]. After a determined time, the rotation of the container stops, and the semi-solid slurry discharges from its bottom. It is based on heat exchange surrounding the mold and the slurry [14]. In other words, the purpose of this method is to reduce the thermal gradient from the center to the mold wall [12,13]. The results of other studies show that by decreasing the thermal gradient, the number of effective nuclei has increased [15,16]. Research by DOHERTY and VOGEL [15] shows that by applying shear stress to a semi-solid slurry and creation effective fluid flow, the thermal and concentration gradients decrease, and the number of nucleation sites increases. According to the results of research related to semi-solid processes [17−20], the solid fraction is the most important factor influencing the thixotropic behavior of semi-solid slurries. In other words, the effect of the rotational speed and the applied shear force on the semi-solid slurry is highly dependent on the solid fraction. To find out and analyze this relationship, it is necessary to calculate the solid fraction in the semi-solid process. For this purpose, cooling curve thermal analysis was applied to interpreting the solidification parameters [20−24].

Computer-aided cooling curve thermal analysis, CA-CCTA, is one of the prevalent methods of thermal analysis, which can be used to calculate important solidification characteristics such as solid fraction, cooling rate, phase transformation and nucleation, and dendrite coherency point [21−26]. The cooling curve is obtained by direct and instantaneous measurement of temperature changes as function of time, from the beginning of the solidification to the end of the process [22,27,28]. The relationship between the cooling rate and the parameters of the semi-solid process can also be investigated.

Effect of Al content and cooling rate on solidification characteristics of AZ magnesium alloys was investigated by YAVARI and SHABESTARI [29] using CA-CCTA. The results showed that the nucleation temperature of the primary $\alpha$-Mg phase increased by cooling rate. The heat extraction rate has caused this change. In this point of view, decreasing the cooling rate decreases the heat extraction, and the molten alloy is cooled to a lower temperature than the equilibrium melting point. This condition leads to more potential substrates to nucleate because of the existing appropriate undercooling. Therefore, nucleation is continued easily and quickly [28,29]. But some researchers have reported reduction in nucleation temperature by increasing the cooling rate. They proposed that kinetics of diffusion is responsible for reduction in nucleation temperature [29].

It has been reported that the nucleation and growth temperature of the eutectic phases ($\alpha$-Mg + $Mg_{17}Al_{12}$) decreased by increasing the cooling rate. Therefore, the morphology of the eutectic phases changed from continuous coarse at the grain boundary to finer and more dispersed particles in AZ91 magnesium alloy [29]. Dendrite coherency point (DCP) makes a significant contribution in solid fraction changes. During solidification and before this point, the growth of dendrites continues freely, and melt feeding completes among the slurry. After this point, growth of the dendritic network causes the appearance of solid-state properties such as thermal conductivity, shear strength and shrinkage; and development of the casting defects is the final result of this behavior [26−30].

In the present study, rotating container process (RCP) has been designed based on SEED process to investigate the effects of shearing forces caused by the rotational speed of the container, the temperature of semi-solid slurry, and solid fraction on the grain morphology. Solidification parameters and microstructure of AZ91 and AZ91−1Ca (wt.%) magnesium alloys produced in RCP process has also been investigated.

## 2 Experimental

### 2.1 Materials

In this study two kinds of magnesium alloy, AZ91 and AZ91−1Ca were used. Magnesium ingots with high purity of 99.9 wt.%, were melted in a steel crucible under protection of anti-oxidation flux and inert argon gas atmosphere at 720 °C. Then, pure alloying elements including Al and Zn, were added to the molten alloy and Ca was added in the form of Al−10Ca master alloy. Stirring stage began after holding for 10 min. Then, it was poured into a preheated steel mold. The chemical composition of the AZ91 and AZ91−1Ca alloys is presented in Table 1.

**Table 1** Chemical composition of AZ91 and AZ91−1Ca alloys (wt.%)

| Alloy | Al | Zn | Ca | Cu | Fe | Si | Mg |
|---|---|---|---|---|---|---|---|
| AZ91 | 9.12 | 1.06 | − | 0.09 | 0.03 | 0.02 | Bal. |
| AZ91−1Ca | 8.96 | 0.94 | 0.98 | 0.08 | 0.03 | 0.02 | Bal. |

### 2.2 Semi-solid casting in rotating container process (RCP)

400 g AZ91 magnesium alloy was melted in a cylindrical steel container in a resistance furnace at 660 °C for 40 min under protection of the anti-oxidizing flux and argon gas atmosphere. The container was quickly removed from the furnace and mounted on the circular plate after complete melting. The rotation of the container began at certain speeds as the temperature was reduced to 640 °C. The temperature of the melt was measured using a K-type thermocouple and recorded continuously during the rotation. Inert argon gas with the pressure of 500 Pa was purged on the melt during the rotation, and as the melt temperature decreased to the specified temperature, the rotation stopped and the container quickly removed from the rotating circular plate. Then, the semi-solid slurry was poured into a 200 °C preheated cylindrical steel mold with the dimensions of 100 mm in height and 30 mm in diameter. The same procedure was also performed for AZ91−1Ca alloy.

It is worth mentioning that the rotation speed of the container was controlled by an electrical inverter. The actual rotation speed of the container was measured by a laser counter and the electrical inverter was calibrated based on that. In this work, the rotation speeds of the container were 150, 180 and 210 r/min, and the operating temperatures were 595, 590, 585 and 580 °C, based on the range of solid fraction. These temperatures were in accordance to the end of the rotation.

### 2.3 Thermal analysis during RCP process

It is important to determine the solidification range and solid fraction as a function of temperature in the semi-solid state. Therefore, computer aided cooling curve thermal analysis (CA-CCTA) was used to record the exact temperature of the melt and the solid fraction during applying shearing forces into the melt caused by the rotational speed of the container.

K-type (chromel-alumel) thermocouple produced by OMEGA Engineering Company was linked to an Analog/Digital converter (high-speed data acquisition system) connected to a computer. The A/D converter used in this experiment was ADAM−4018 and had a sensitive 16-bit (resolution of 1/216 or 0.0015%) microprocessor-controlled sigma-delta A/D converter; response time of 0.02 s, high accuracy detection and having 8-channel analog input module that provides programmable input ranges on all channels [31]. Before this stage the thermocouples were calibrated using a molten high purity aluminum.

Data recording with the frequency of 10 $s^{-1}$ was performed. The analog-to-digital (A/D) converter received the data from the thermocouples, which were in the form of voltage changes in the range of a few millivolts, and transmitted it to the converter card via the interface wires. The data were analyzed and the curves were plotted using Origin pro 9.0 software (Origin Lab Corporation, Northampton, MA). The adjacent averaging method was used to smooth the thermal analysis curves.

Thermocouples were inserted in the two separated copper tubes, and were supported by a stand and fixed one in the center and the other near the wall of the melt container. Thermal analysis was performed during rotation of the melt container with the above-mentioned rotational speeds at different operating temperatures (solid fraction).

The rotation of the melt container began at a temperature of 640 °C. To investigate the entire range of temperatures, the rotation continued until the temperature of the slurry was reduced to 579 °C. After the rotation was finished, the temperature was recorded until 400 °C. Thermal analysis was also performed in the conventional casting with the same condition without any rotation (0 r/min) to compare its result with the results of the samples that were produced in the rotating container. The schematic of the thermal analysis system is shown in Fig. 1.

According to the pervious study [31], cooling rate during thermal analysis tests can be calculated from the slope of cooling curve, $\Delta T/\Delta t$, at the temperature interval between liquidus point and eutectic reaction. Dendrite coherency measurements were carried out using two-thermocouple thermal analysis during continuous cooling. Locations of

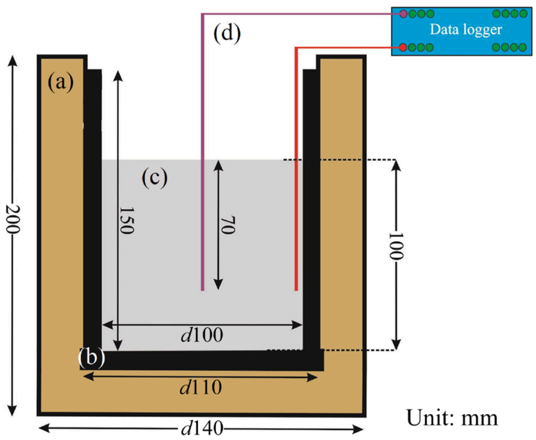


**Fig. 1** Schematic of thermal analysis system: (a) Thermal insulation; (b) Container; (c) Semi-solid slurry; (d) Thermocouple

the thermocouples were in the center and adjacent the inner wall of the melt container.

The curves of solidification characteristics such as solid fraction were plotted after the calculation of the temperature between the wall and the central regions of the container ($\Delta T = T_W - T_C$) for each sample. Characteristics of dendrite coherency point including solid fraction ($f_s^{DCP}$), temperature ($T_{DCP}$) and time ($t_{DCP}$) were calculated. In this study, quantification of the solid fraction is based on the Newtonian model used by some researchers to plot the curves [23,24,26−28,32].

### 2.4 Microstructural evaluations

All samples were produced from RCP experiments and conventional casting (0 r/min), and sectioned horizontally through the place that the tip of the thermocouples was located. According to the pervious study [31], the samples were prepared for metallographic study after grinding, polishing, and etching with 2% nital (1 mL $HNO_3$ + 49 mL $C_2H_5OH$) and acetic picral (60 mL $CH_3COOH$ + 30 mL $H_2O$ + 12 g picric acid + 200 mL $C_2H_5OH$) to reveal microstructure and macrostructure, respectively. The grain structures were observed using HUVITZ−HM25 optical microscope. For each sample, three pictures were taken from central zone and the grain size was evaluated for every picture based on linear intercept method described in ASTM standard E112—88. Circularity of grain was measured using Clemex vision PE 3.5 software (Clemex Technologies Inc., Longueil, Quebec, Canada) for each sample.

## 3 Results and discussion

### 3.1 Cooling curves

The cooling curves of AZ91 and AZ91−1Ca alloys performed at the rotation speeds of 0, 150, 180 and 210 r/min are shown in Fig. 2. The cooling curve and its first derivative curve of the alloys at the rotational speed of 210 r/min of the melt container are shown in Fig. 3. The data of these curves are obtained from the thermocouple which was located in the center of the rotating container.

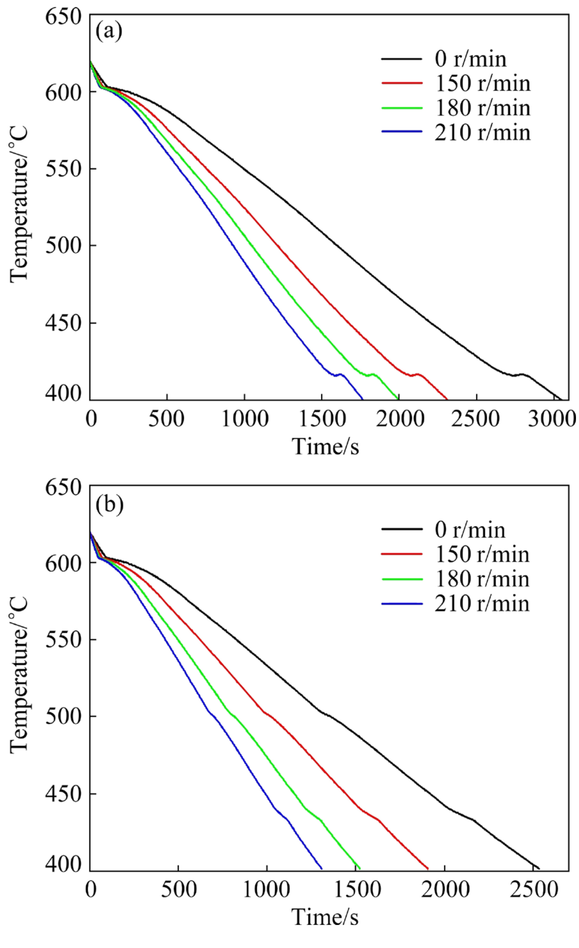


**Fig. 2** Cooling curves of samples at different rotation speeds of RCP for both alloys: (a) AZ91; (b) AZ91−1Ca

The first peak in the first derivative curve refers to nucleation and growth of the primary $\alpha$-Mg phase ($T_{N,\alpha}$). The release of latent heat during the formation of the primary $\alpha$-Mg phase and the growth of this phase cause a sharp increase in this peak. The last peak on the first derivative curve indicates the nucleation and growth of ($\alpha$-Mg + $Mg_{17}Al_{12}$) eutectic phases, which is the last transformation during the solidification in these

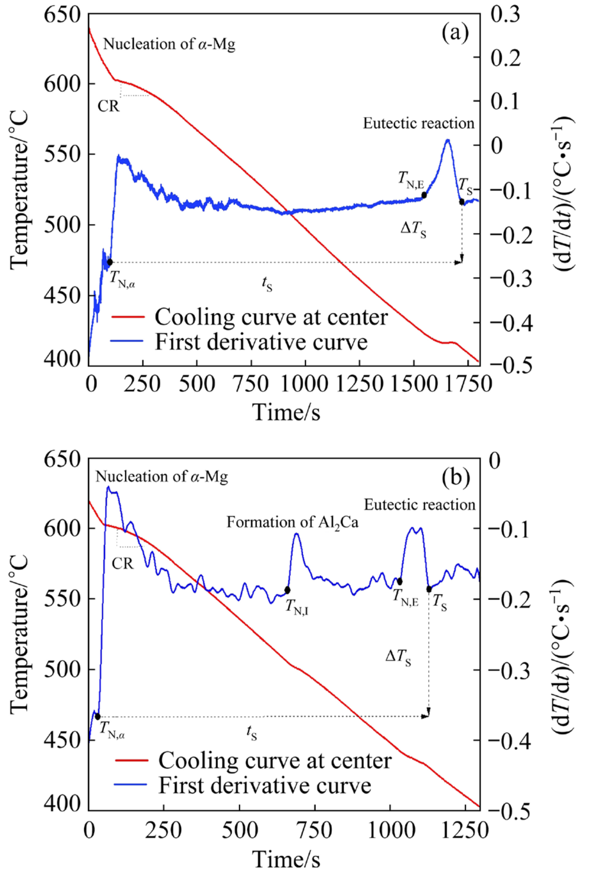


**Fig. 3** Cooling curves and first derivative curves at rotation speed of 210 r/min for both alloys: (a) AZ91; (b) AZ91−1Ca

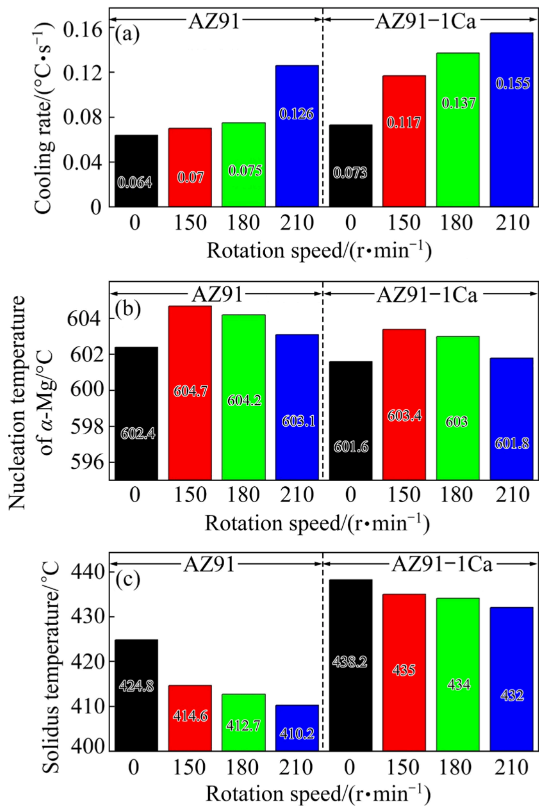


**Fig. 4** Effect of rotation speed and addition of 1 wt.% Ca on solidification characteristics: (a) Cooling rate; (b) Nucleation temperature of $\alpha$-Mg; (c) Solidus temperature

alloys ($T_S$). Therefore, $\Delta T_S(=T_{N,\alpha}-T_S)$ and $t_S$ are the temperature of solidification range and solidification time, respectively. In the cooling curve and first derivative curve of alloy AZ91−1Ca, the formation peak of $Al_2Ca$ was detected in the temperature range of 505−510 °C due to the presence of 1 wt.% Ca in this alloy (Fig. 3(b), $T_{N\text{-}I}$). The formation of this phase in this temperature range has also been reported [33].

Solidification characteristics of AZ91 and AZ91−1Ca alloys at different rotational speeds are shown in Figs. 4 and 5. The cooling rate in both alloys increased by increasing the rotation speed (Fig. 4(a)). The nucleation temperature changes of the $\alpha$-Mg primary phase are shown in Fig. 4(b). The nucleation temperature of this phase ($T_{N,\alpha}$) is increased by about 2.3 °C in both alloys at a rotation speed of 150 r/min. Researchers have proposed two mechanisms to explain this behavior. The first mechanism indicates the effect of increasing the cooling rate on reducing the diffusion rate and thus reducing the nucleation temperature of the primary phase [30]. While, the second mechanism points out an increase in nucleated clusters by increasing the cooling rate and causes an increase in nucleation temperature [28,29].

The addition of 1 wt.% Ca to the AZ91 alloy reduced the nucleation temperature ($T_{N,\alpha}$) by about 1.3 °C. The reason can be attributed to the reduction of the cooling rate in the presence of Ca. However, both the rotation speed and the addition of 1 wt.% Ca have little effect on the nucleation temperature of the $\alpha$-Mg primary phase.

The solidus temperature ($T_S$) in RCP operations decreased to a minimum of 10.2 °C and a maximum of 14.6 °C in AZ91 alloy. It decreased to a minimum of 2.8 °C and a maximum of 5.8 °C in AZ91−1Ca alloy. The results show that the rotation speed of the container on the solidus temperature ($T_S$) of the alloys is more effective compared to $T_{N\text{-}\alpha}$ (Fig. 4(c)). This behavior is attributed to the higher diffusion coefficient of the alloying elements in the melt than in the solid. It seems that by increasing cooling rate, the diffusion

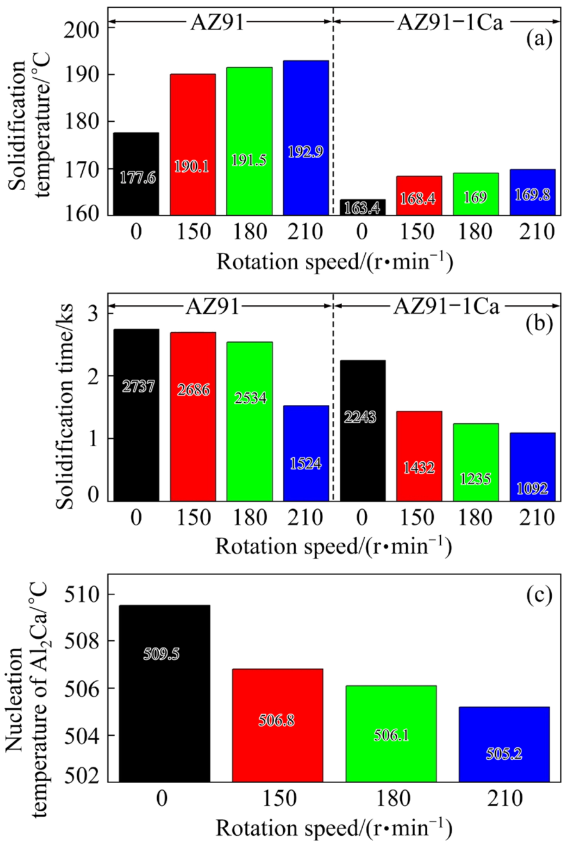


**Fig. 5** Effect of rotation speed and addition of 1 wt.% Ca on solidification characteristics: (a) Solidification temperature; (b) Solidification time; (c) Nucleation temperature of $Al_2Ca$

rate of the alloying elements such as aluminum in the semi-solid region decreases and delays the formation of the eutectic phases ($\alpha$-Mg + $Mg_{17}Al_{12}$). Also, increasing cooling rate reduces the formation temperature of the eutectic phases, which is actually the solidus temperature ($T_S$). The number of nucleation sites of $\beta$-$Mg_{17}Al_{12}$ intermetallic phase increases with increasing the cooling rate. Therefore, it can be concluded that increasing the cooling rate reduces the temperature of the final phase formation.

The addition of 1 wt.% Ca to AZ91 alloy increased the solidus temperature ($T_S$) at all rotation speeds (Fig. 4(c)). However, this increased amount in the samples obtained from RCP is more than the as-cast sample (0 r/min). The solidus temperature was increased by 20.4, 21.3 and 21.8 °C, in samples with rotation speeds of 150, 180 and 210 r/min, respectively. While, this increase is 13.4 °C in the as-cast sample. Since the presence of Ca up to 1 wt.% reduces the amount of $\beta$-$Mg_{17}Al_{12}$ phase [33], it can be concluded that in samples at the rotation speeds of 150, 180 and 210 r/min, a large drop in solidus temperature, which might be caused by RCP, has been prevented.

Figure 5(a) shows the effect of the rotation speed of the container on the solidification range ($\Delta T_S=T_{N,\alpha}-T_S$) of AZ91 and AZ91−1Ca alloys. The temperature of solidification for AZ91 alloy is 177.6 °C in the as-cast sample (0 r/min). It increases by about 15.3 °C with increasing the speed of the container to 210 r/min. The addition of 1 wt.% Ca reduces $\Delta T_S$ at all rotation speeds, which is related to having a greater effect on $T_S$ than $T_{N,\alpha}$. The solidification time ($t_S$) decreases in both alloys as a function of cooling rate (Fig. 5(b)). The solidification time is reduced by about 45% (from 2737 to 1524 s) compared to the 0 r/min sample. In AZ91−1Ca alloy, the solidification time decreases drastically at 150 r/min due to cooling rate. It is worth mentioning that the time of solidification in all samples increased significantly and observed in a range of 2737−1092 s compared to the conventional casting due to the usage of thermal insulation in this study. As shown in Fig. 3(b), the addition of 1 wt.% Ca caused a peak in the cooling curve in the range of 505−510 °C. This peak is related to the formation of the $Al_2Ca$ intermetallic phase. The nucleation temperature changes ($T_{N,I}$) of this phase are shown in Fig. 5(c). The nucleation temperature of this phase is 509.5 °C in as-cast condition (0 r/min), which decreases to 505.2 °C at the rotation speed of 210 r/min.

### 3.2 Solid fraction

The solid fraction was calculated based on the area under the first derivative curve to the reference curve. Since the temperature was investigated in the range of 605−580 °C, the solid fraction changes are plotted for both alloys in Fig. 6 in this temperature range.

As shown in Fig. 6(a), in the AZ91 alloy by decreasing temperature from 600 to 595 °C, a sharp increase in the solid fraction is observed in the samples obtained by applying shearing forces, compared to the as-cast sample (0 r/min). The reason seems to be the increase in the number of nuclei formed in the melt due to the forced fluid flow and the increase in the rate of heat output from the rotating container, and creating suitable conditions for the nuclei to remain stable. The

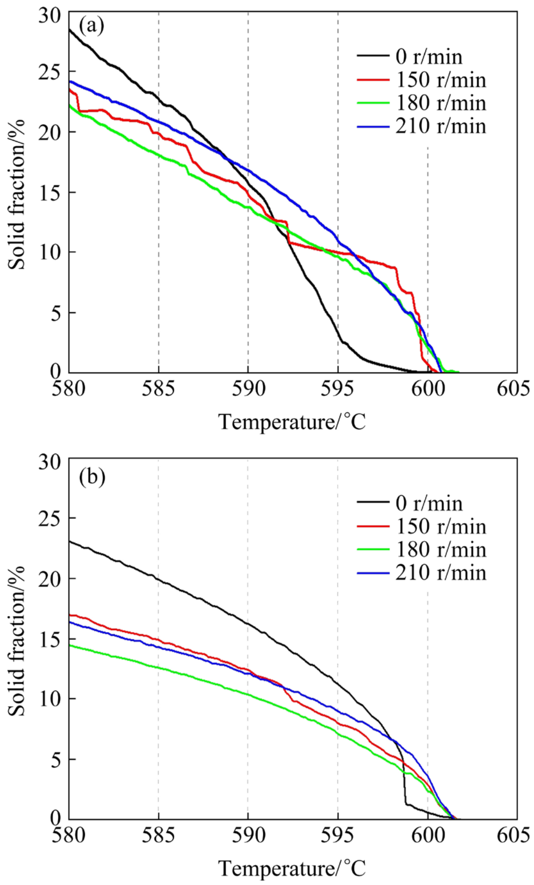


**Fig. 6** Solid fraction as function of temperature at different rotation speeds for alloys: (a) AZ91; (b) AZ91−1Ca

semi-solid RCP method is based on creating constant thermal and concentration gradient throughout the slurry. FAN [10] and DOHERTY and VOGEL [15] reported that by applying shearing forces to a semi-solid slurry, the heterogeneous nucleation and the nucleation frequency increased. In RCP method, the fluid flow creates heterogeneous nucleation and an increase in number of nuclei. By decreasing temperature from 595 °C, the slope of the solid fraction curve is much higher in the sample without any shearing force (0 r/min). This behavior is due to the shear force and the creation of forced fluid flow in the slurry. By creation of forced convection, the melt trapped between the clusters and the dendritic network is decreased during the growth stage, resulting in a more homogeneous composition of the melt and decrease in growth rate of the clusters and the dendritic network. The trend of changes in the range of 595−580 °C shows that the lowest solid fraction is obtained by applying shear force at a rotation speed of 180 r/min and the highest solid fraction is obtained by applying shear force at a rotation speed of 210 r/min (Fig. 6(a)). The reason for this behavior could be attributed to a turbulent flow at a rotation speed of 210 r/min in the slurry.

Figure 6(b) shows the solid fraction changes in the same temperature range for the AZ91−1Ca alloy. The solid fraction in the samples with rotation is lower than that without any rotation. This difference increases with decreasing operational temperature. The addition of 1 wt.% Ca causes uniform changes in the samples produced with the rotation. Therefore, the difference between the solid fraction values of the 0 r/min sample and the other samples increases compared to the AZ91 alloy. The sample with the rotation speed of 180 r/min has the lowest solid fraction due to the balance between the cooling rate and the forced fluid flow.

Figure 7(a) shows the solid fraction as a function of rotation speed at different temperatures for AZ91 alloy. The solid fraction increased by 13.2% in the temperature range of 595−580 °C at a rotation speed of 150 r/min. The solid fraction increases by 12.65% at a rotation speed of 180 r/min. Finally, the solid fraction increased by 13.2% (from 11.3% to 24.5%) at the highest rotation speed of 210 r/min. Figure 7(b) shows the same changes for the AZ91−1Ca alloy. The solid fraction increased by 9% (from 8.2% to 17.2%) in the temperature range of 595−580 °C with a rotation speed of 150 r/min. The solid fraction increased by 6.6% (from 7.5% to 14.1%) at a rotation speed of 180 r/min. Finally, the solid fraction increased by 8.9% (from 8.1% to 17%) at the highest rotation speed of 210 r/min.

Two conclusions can be drawn from the comparison of the results of Figs. 6 and 7. Firstly, the addition of 1 wt.% Ca to AZ91 reduced the solid fraction at the similar points during RCP. Results of the similar research [4,33] show that the addition of Ca to the AZ91 alloy forms $\beta$-phase and final eutectic ($\alpha$-Mg+$Mg_{17}Al_{12}$) phases discontinuously. Therefore, the ratio of the surface to the volume of the feeding channels increased, which makes the feeding more difficult. As a result, the solid fraction is reduced due to the reduced melt feeding. Secondly, the addition of 1 wt.% Ca caused the convergence of solidification characteristics in the semi-solid process compared to the 0 r/min sample. It reduced the difference in solidification characteristics at 210 and 150 r/min compared to 180 r/min of rotation speed.

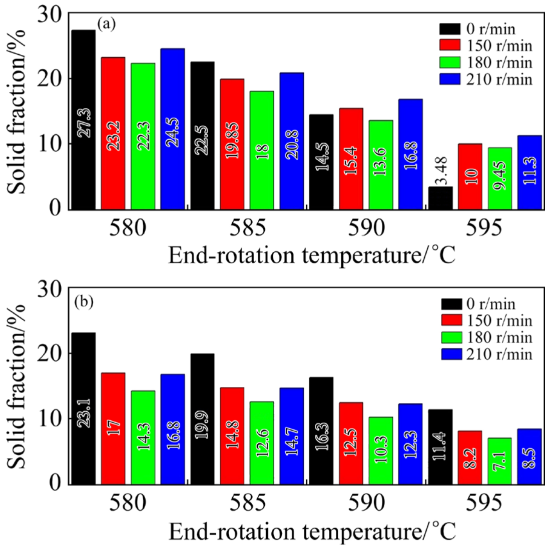


**Fig. 7** Solid fraction as function of rotation speed in RCP for alloys: (a) AZ91; (b) AZ91−1Ca

### 3.3 Dendrite coherency point

To determine dendrite coherency point (DCP), data were obtained from two thermocouples located in the center and near the wall of the rotating container. The largest temperature difference between the center and the wall occurs when the dendritic network is cohesive [27]. The importance of identifying the coherency point of dendrites in semi-solid processes is that the shear strength of the semi-solid slurry increases strongly at this point [27]. The curves of cooling, solid fraction, and melt temperature difference between center and wall of the rotating container, for AZ91-180 r/min and AZ91−1Ca-180 r/min alloys are shown in Fig. 8. Also, changes in DCP characteristics, including solid fraction, temperature, and time, for all 8 samples are presented in Fig. 9.

According to Fig. 8, it can be concluded that the rotation of the container at all speeds of 150, 180 and 210 r/min is completed before DCP. This indicates that the end-rotation temperature was selected correctly and there were suitable conditions for applying a shear force to the semi-solid slurry. The coherency temperature of the dendrites ($T_{DCP}$) in both alloys decreased by applying the rotation. Therefore, in the AZ91 alloy, $T_{DCP}$ changed from 585 °C in the sample without rotation to 560.4 °C in the sample with 210 r/min (Fig. 8(a)). This change in AZ91−1Ca alloy is from 580 to 556.6 °C. The reason for this reduction can be attributed to the rotation speed and the cooling rate (Fig. 4(a)). As the rotation speed increases, the cooling rate also increases, which affects the diffusion kinetics in the semi-solid slurry. As the cooling rate increases, the time required to complete the diffusion process to create a dendritic network is limited. Therefore, the required temperature for dendritic coherency is delayed and reduced.

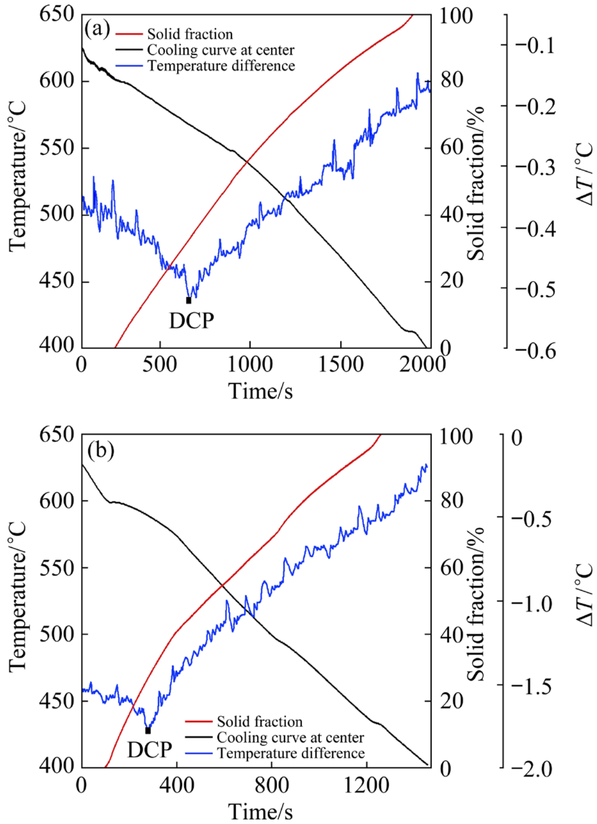


**Fig. 8** Curves of melt temperature difference between center and wall of rotating container ($\Delta T=T_C-T_W$), solid fraction and cooling curve during solidification in RCP process at rotation speed of 180 r/min for alloys: (a) AZ91; (b) AZ91−1Ca

The changes of the solid fraction at DCP ($f_{DCP}$) as a function of the rotation speed, are presented in Fig. 8(b). It shows that the solid fraction at DCP increased in both alloys by applying the rotation. $f_{DCP}$ increased from 26.3% at 0 r/min to 39.8% at 210 r/min in AZ91 alloy, and it increased from 22.6% at 0 r/min to 30.2% at 210 r/min in AZ91−1Ca alloy. The linear growth rate of dendrites increased with increasing rotation speed and consequently increasing cooling rate. This is because the time required to complete the diffusion of the elements is reduced, creating a concentration gradient in the inter-dendritic regions, and causes the melt near the growing dendritic arms achieves faster to the average chemical composition. It has

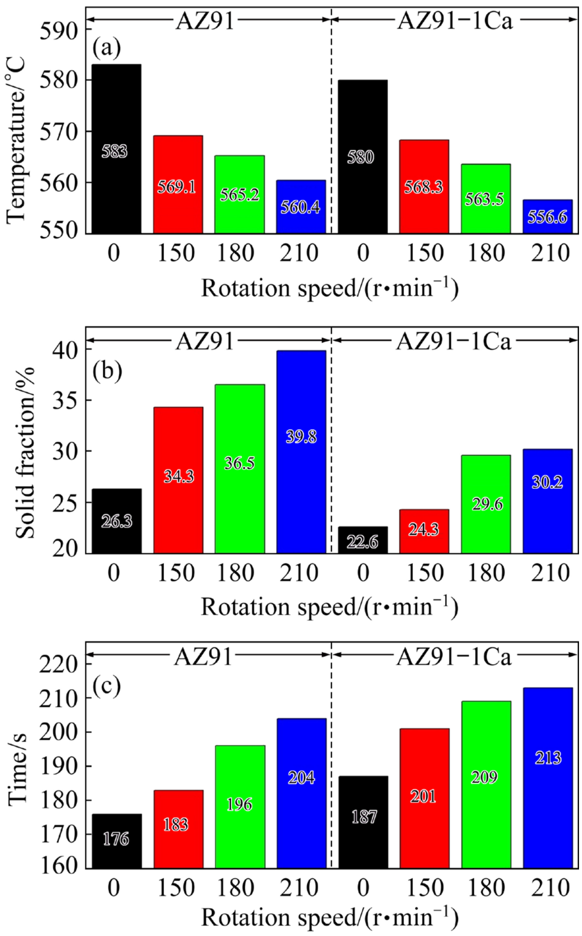


**Fig. 9** Effect of RCP and addition of 1 wt.% Ca on characteristics of DCP: (a) Temperature; (b) Solid fraction; (c) Time

been reported that the lateral growth rate of dendrites has increased, which increases the solid fraction until the dendrites coherency is reached [27,34].

Figure 8(c) shows the trend of time of DCP ($t_{DCP}$) as a function of the rotation speed in both alloys. It increases from 176 s at 0 r/min to 204 s at 210 r/min in AZ91 alloy, and it also increases from 187 s at 0 r/min to 213 s at 210 r/min in AZ91−1Ca alloy. The reason for this behavior can be attributed to the greater effect of forced fluid flow than the cooling rate (solid fraction section). By applying the rotation, creating a forced fluid flow reduces the concentration gradient in the inter-dendritic areas and thus increases the chance of achieving dendritic coherency [33]. Creating a laminar fluid flow (non-turbulent) prevents the formation of any effective concentration gradient in front of the solidification zone. Therefore, it is expected that the growth rate of dendrites and the time required for colliding the tip of the dendrites to form a dendritic network, will increase. The addition of 1 wt.% Ca to AZ91 alloy altered all three parameters of $f_{DCP}$, $T_{DCP}$ and $t_{DCP}$ in all conditions of RCP. The maximum changes were −9.6%, −3.4 °C and 18 s, respectively. In fact, it delayed the occurrence of DCP along with reducing the solid fraction. Decreasing the solid fraction at DCP ends the volumetric feeding. The effect of this behavior has been investigated in the microstructural studies, where grain size is expected to be modified due to the delay in the occurrence of DCP.

### 3.4 Microstructural evaluation

Figure 10 shows the phases in the microstructure of AZ91 and AZ91−1Ca alloys without applying rotation. Microstructure consists of the $\alpha$-Mg phase, and $Mg_{17}Al_{12}$ intermetallic phase, which are observed in light and dark contrast, respectively. Also, $Al_2Ca$ intermetallic phase is observed in the microstructure of AZ91−1Ca alloy. Grain structure of both alloys without any rotation, and optimum condition of rotation speed of 180 r/min and the end of operating temperature of rotation of 585 °C, are shown in Fig. 11.

The objectives of the research in the semi-solid process and the addition of 1 wt.% Ca to AZ91 alloy are to improve the globularity (circularity) and to modify the grain size, respectively. Therefore, the average of circularity for all samples at different rotation speeds of the container and various operating temperature for AZ91 alloy, and the optimum condition of rotation speed of 180 r/min and the operating temperature of 585 °C for AZ91−1Ca, are shown in Fig. 12. In the optimum condition of a rotation speed of 180 r/min and the operating temperature of 585 °C, the best circularity for AZ91 and AZ91−1Ca is 0.72 and 0.81, respectively.

A dendritic microstructure is observed in 0 r/min samples and their circularity factor is low. However, under this condition, the addition of 1 wt.% Ca to AZ91 alloy increases the circularity factor from 0.12 to 0.17. This microstructural improvement is shown in Figs. 11(a) and (b). As the rotation speed increases to 150 r/min, the circularity factor of the grains increases very slightly to a maximum of 0.23, indicating that this speed is not sufficient to achieve a globular microstructure. This result is in a good agreement with the results of

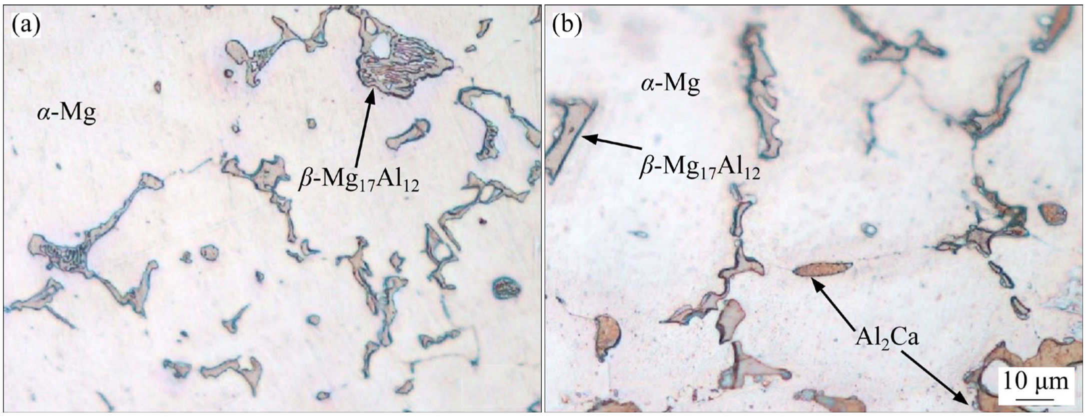


**Fig. 10** Microstructure of both alloys at 0 r/min: (a) AZ91; (b) AZ91−1Ca

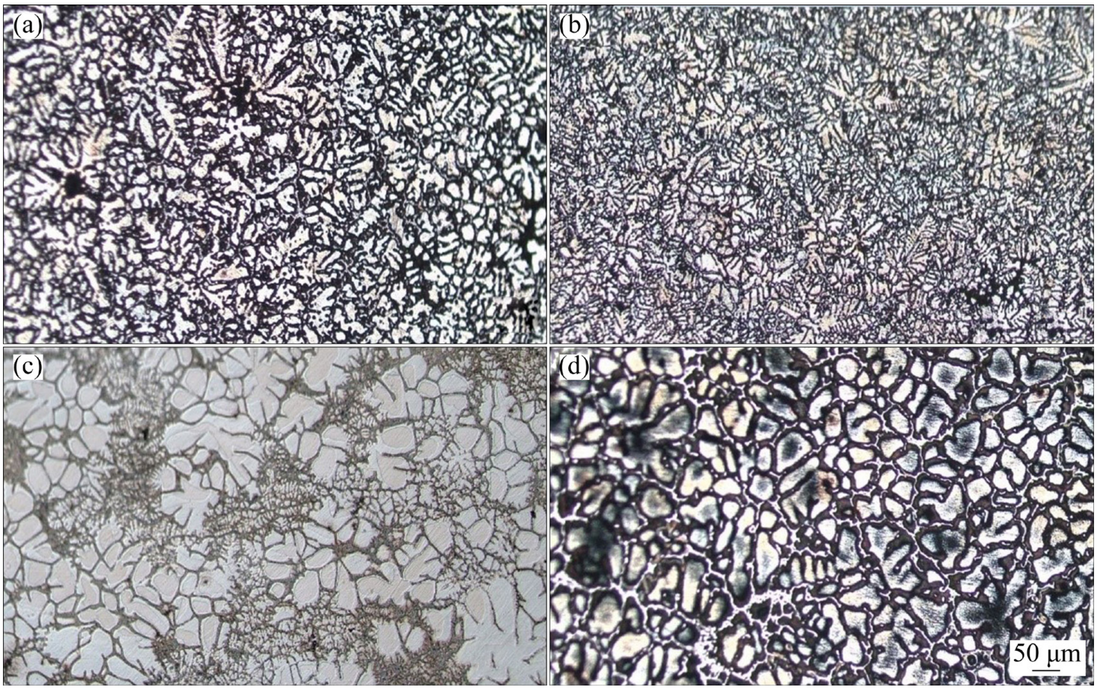


**Fig. 11** Effect of RCP and addition of 1 wt.% Ca at operating temperature of 585 °C with 0 r/min (a, b) and 180 r/min (c, d): (a, c) AZ91; (b, d) AZ91−1Ca

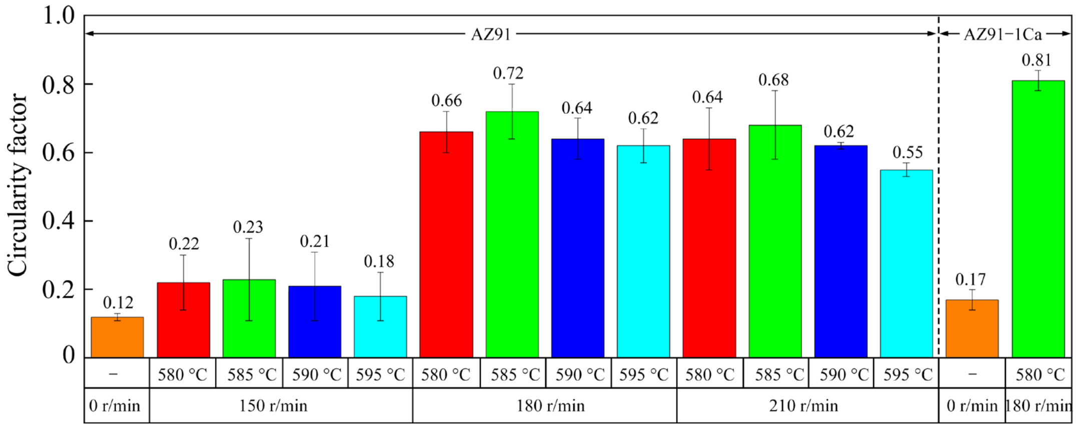


**Fig. 12** Effect of RCP and addition of 1 wt.% Ca to AZ91 alloy on circularity factor of samples

thermal analysis. No effective fluid flow is created at this rotation speed to affect the growth of clusters and dendritic network. Therefore, morphological change to the globular state did not occur. Circularity factor increases at the rotation speeds of 180 and 210 r/min and non-dendritic morphology is observed in the microstructure of the alloys. According to Figs. 6 and 7, the solid fraction at 180 r/min is lower than that of 210 r/min. This is because of the result of a balance between the cooling rate and the forced fluid flow. The higher circularity factor at a rotation speed of 180 r/min than that at 210 r/min, shows the effect of the balance of these two effective factors. Because, the equilibrium of both of them occurs at 180 r/min. The solid fraction decreases and the effect of RCP on the thermal gradient also decreases. Therefore, the microstructure changes to a more globular morphology. By further reducing the rotation temperature to 580 °C, because of a sharp increase in the solid fraction according to Fig. 7, the effect of the forced fluid flow on the growth of the clusters is limited due to the high density of the dendritic network. Therefore, the circularity factor is reduced at 580 °C compared to 585 °C, at both rotation speeds of 180 and 210 r/min.

The appropriate effects of RCP and improvement of the microstructure due to the addition of 1 wt.% Ca to AZ91 alloy were observed simultaneously in AZ91−1Ca alloy with 180 r/min at 585 °C. Therefore, in the optimum condition of 180 r/min and 585 °C, in AZ91 alloy, the circularity factor is 0.72 and the grain size is 73.4 μm, and in AZ91−1Ca alloy, the circularity factor is 0.81 and the grain size is 53.2 μm.

## 4 Conclusions

(1) The cooling rate of both alloys, was significantly increased by about 3 times at 210 r/min compared to that at 0 r/min.

(2) At a rotation speed of 180 r/min, the balance between two influencing factors of the cooling rate and forced fluid flow, resulted in a minimum solid fraction compared to the other rotational speeds.

(3) The temperature of DCP decreased to 22.7 °C in the AZ91 and 23.4 °C in the AZ91−1Ca alloy, respectively, due to the reduction of diffusion rate.

(4) The solid fraction at DCP of AZ91 alloy increased to 39.8% at a rotation speed of 210 r/min, due to increasing linear and lateral growth of dendrites.

(5) By adding Ca, the solid fraction at DCP reduced at a constant rotation speed and caused the conversion of volumetric to interdendritic feeding in the semi-solid slurry.

(6) Microstructural studies revealed that the optimum conditions of this semi-solid process, were a rotation speed of 180 r/min and a temperature of 585 °C. The globular morphologies with the circularity factor of 0.72 and 0.81, and grain size of 73.4 and 53.2 μm, are obtained in AZ91 and AZ91−1Ca alloys, respectively.

## References

[1] CHANG Z Y, SU N J, WU Y, LAN Q, PENG L M, DING W J. Semisolid rheoforming of magnesium alloys: A review [J]. Materials & Design, 2020, 195: 108−990.

[2] STJOHN D H, EASTON M A, QIAN M, TAYLOR J A. Grain refinement of magnesium alloys: A review of recent research theoretical developments, and their application [J]. Metallurgical and Materials Transactions A, 2013, 44: 2935−2949.

[3] DING Y F, WEN C E, HODGSON P, LI Y C. Effects of alloying elements on the corrosion behavior and biocompatibility of biodegradable magnesium alloys: A review [J]. Journal of Materials Chemistry B, 2014, 2: 1912−1933.

[4] YIM C D, KIM Y M, YOU B S. Effect of Ca addition on the corrosion resistance of gravity cast AZ31 magnesium alloy [J]. Materials Transactions, 2007, 48: 1023−1028.

[5] HIRAI K, SOMEKAWA H, TAKIGAWA Y, HIGASHI K. Effects of Ca and Sr addition on mechanical properties of a cast AZ91 magnesium alloy at room and elevated temperature [J]. Materials Science and Engineering: A, 2005, 403: 276−280.

[6] BAGHNI I M, WU Y S, LI J Q, DU C W, ZHANG W. Mechanical properties and potential applications of magnesium alloys [J]. Transactions of Nonferrous Metals Society of China, 2003, 13: 1253−1259.

[7] PEKGULERYUZ M O, KAYA A. Creep resistant magnesium alloys for powertrain applications [J]. Advanced Engineering Materials, 2003, 5: 866−878.

[8] WU G H, FAN Y, GAO H T, ZHAI C Q, ZHU Y P. The effect of Ca and rare earth elements on the microstructure mechanical properties and corrosion behavior of AZ91D [J]. Materials Science and Engineering: A, 2005, 408: 255−263.

[9] LI S S, TANG B, ZENG D B. Effects and mechanism of Ca on refinement of AZ91D alloy [J]. Journal of Alloys and Compounds, 2007, 437: 317−321.

[10] FAN Z. Semisolid metal processing [J]. International Materials Reviews, 2002, 47: 49−85.

[11] KLEINER S, BEFFORT O, WAHLEN A, UGGOWITZER P J. Microstructure and mechanical properties of squeeze cast and semi-solid cast Mg–Al alloys [J]. Journal of Light Metals, 2002, 2: 277−280.

[12] NAFISI S, GHOMASHCHI R. Semi-solid processing of aluminum alloys [M]. Amsterdam: Springer International Publishing, 2016.

[13] LANGLAIS J, LEMIEUX A. The SEED technology for semi-solid processing of aluminum alloys: A metallurgical and process overview [J]. Solid State Phenomena, 2006, 116/117: 472−477.

[14] NAFISI S. Effects of grain refining and modification on the microstructural evolution of semi-solid 356 alloy [M]. Quebec: University of Quebec, 2006.

[15] DOHERTY R, VOGEL A. Stir-cast microstructure and slow crack growth [J]. Solidification and Casting of Metals, 1977, 1: 518−525.

[16] JOLY P A, MEHRABIAN R. The rheology of a partially solid alloy [J]. Journal of Materials Science, 1976, 11: 1393−1418.

[17] BOLOURI A, ZHAO Q F, CÔTÉ P, CHEN X G., Microstructure and rheological properties of semi-solid 7075 slurries using SEED rheocasting process [J]. Solid State Phenomena, 2016, 256: 288−293.

[18] JANUDOM S, WANNASIN J, BASEM J, WISUTMETHANGOON S. Characterization of flow behavior of semi-solid slurries containing low solid fractions in high-pressure die casting [J]. Acta Materialia, 2013, 61: 6267−6275.

[19] BURAPA R, JANUDOM S, CHUCHEEP T, CANYOOK R, WANNASIN J. Effects of primary phase morphology on mechanical properties of Al−Si−Mg−Fe alloy in semi-solid slurry casting process [J]. Transactions of Nonferrous Metals Society of China, 2010, 20(S): s857−s861.

[20] ZHANG Y, WU G H, LIU W C, ZHANG L, PANG S, DING W J. Preparation and rheo-squeeze casting of semi-solid AZ91−2wt.%Ca magnesium alloy by gas bubbling process [J]. Journal of Materials Research, 2015, 30: 825−832.

[21] SHABESTARI S G, GHODRAT S. Assessment of modification and formation of intermetallic compounds in aluminum alloy using thermal analysis [J]. Materials Science and Engineering: A, 2007, 467: 150−158.

[22] MALEKAN M, SHABESTARI S G. Computer-aided cooling curve thermal analysis used to predict the quality of aluminum alloys [J]. Journal of Thermal Analysis and Calorimetry, 2011, 103: 453−458.

[23] FARAHANY S, OURDJINI A, IDRIS M H, SHABESTARI S G. Computer-aided cooling curve thermal analysis of near eutectic Al−Si−Cu−Fe alloy [J]. Journal of Thermal Analysis and Calorimetry, 2013, 114: 705−717.

[24] EMADI D, WHITING L V, DJURDJEVIC M, KIERKUS W T, SOKOLOWSKI J. Comparison of Newtonian and Fourier thermal analysis techniques for calculation of latent heat and solid fraction of aluminum alloys [J]. Metallurgical and Materials Engineering, 2004, 10: 91−106.

[25] ERBAŞ K C. Analytically solved solid fraction model for the Newtonian thermal analysis of casting [J]. Metallurgical and Materials Transactions A, 2016, 47: 3026−3030.

[26] MOMENI H, SHABESTARI S, RAZAVI S H. Densification and shape distortion of the Al−Cu−Mg pre-alloyed powder compact in super solidus liquid phase sintering process [J]. Iranian Journal of Materials Science and Engineering, 2020, 17: 87−82.

[27] GHONCHEH M H, SHABESTARI S G. Effect of cooling rate on the dendrite coherency point during solidification of Al2024 alloy [J]. Metallurgical and Materials Transactions A, 2015, 46: 1287−1299.

[28] SHABESTARI S G, MALEKAN M. Thermal analysis study of the effect of the cooling rate on the microstructure and solidification parameters of 319 aluminum alloy [J]. Canadian Metallurgical Quarterly, 2005, 44: 305−312.

[29] YAVARI F, SHABESTARI S G. Effect of cooling rate and Al content on solidification characteristics of AZ magnesium alloys using cooling curve thermal analysis [J]. Journal of Thermal Analysis and Calorimetry, 2017, 129: 655−662.

[30] GHONCHEH M H, SHABESTARI S G, ABBASI M H. Effect of cooling rate on the microstructure and solidification characteristics of Al2024 alloy using computer-aided thermal analysis technique [J]. Journal of Thermal Analysis and Calorimetry, 2014, 117: 1253−1261.

[31] YAVARI F, SHABESTARI S G. Assessment of the microstructure, solidification characteristics and mechanical properties of AZ61+$x$Sr magnesium alloys [J]. Metallurgical and Materials Transactions B, 2020, 51: 3089−3097.

[32] MAJHI J, MONDAL A K. Microstructure and impression creep characteristics of squeeze-cast AZ91 magnesium alloy containing Ca and/or Bi [J]. Materials Science and Engineering: A, 2019, 744: 691−703.

[33] LIANG S M, CHEN R S, BLANDIN J J, SUERY M, HAN E H. Thermal analysis and solidification pathways of Mg−Al−Ca system alloys [J]. Materials Science and Engineering: A, 2008, 480: 365−372.

[34] YAVARI F, SHABESTARI S G. Assessment of the effect of cooling rate on dendrite coherency point and hot tearing susceptibility of AZ magnesium alloys using thermal analysis [J]. International Journal of Cast Metals Research, 2019, 32: 85−94.

# 添加钙和转速对旋转容器半固态铸造 AZ91 镁合金显微组织和凝固参数的影响

Saeed G. SHABESTARI, Ehsan GHANIABADI

School of Metallurgy and Materials Engineering,
Iran University of Science and Technology, 1684613114 Tehran, Iran

**摘　要**：采用旋转容器半固态工艺(RCP)和添加 1% Ca(质量分数)对 AZ91 镁合金的显微组织进行改性。在半固态加工过程中进行热分析(CA-CCTA)，以确定合金的显微组织改性与 RCP 参数之间的关系。在 580~640 ℃温度条件下，以 0、150、180 和 210 r/min 的转速旋转装有熔融 AZ91 合金的容器。为了确定合金的凝固特性、固相分数和枝晶搭接点(DCP)，绘制冷却曲线。结果表明，随着转速的增加，冷却速率显著增加，AZ91 和 AZ91−1Ca(质量分数，%)的最大凝固范围分别增加 15.9 和 6.4 ℃。当转速为 180 r/min 时，对浆料施加剪切力可使固相分数最小化并延迟 DCP 的出现。晶粒尺寸和圆形度等显微组织特征也受到影响。在 585 ℃和 180 r/min 条件下可得到圆形度为 0.72、晶粒尺寸为 73.4 μm 的球状组织。在最佳 RCP 条件下，向 AZ91 合金中添加 1% Ca 可使晶粒的圆形度增加到 0.81，晶粒尺寸减小至 53.2 μm。

**关键词**：半固态；镁合金；热分析；剪切力；球状组织

**(Edited by Xiang-qun LI)**